DOI 10.1007/s10891-015-1336-x

Journal of Engineering Physics and Thermophysics, Vol. 88, No. 6, November, 2015

TURBULENT BOUNDARY LAYER ON A FINELY PERFORATED SURFACE UNDER CONDITIONS OF AIR INJECTION AT THE EXPENSE OF EXTERNAL FLOW RESOURCES

V. I. Kornilov, A. V. Boiko, and I. N. Kavun

UDC 532.526.4 + 532.526.72 + 532.546.6

The characteristics of an incompressible turbulent boundary layer on a flat plate with air blown in though a finely perforated surface from an external confined flow through an input device, located on the "idle" side of the plate, have been investigated experimentally and numerically. A stable decrease in the local values of the coefficient of surface friction along the plate length that attains 85% at the end of the perforated portion is shown. The experimental and calculated data obtained point to the possibility of modeling, under earth conditions, the process of controlling a turbulent boundary layer with air injection by using the resources of an external confined flow.

Keywords: *turbulent boundary layer, flat plate, finely perforated surface, blowing-in (injection), input device, friction.*

Introduction. The necessity for energy-saving measures to reduce fuel consumption per passenger-kilometer becomes an increasingly urgent problem of air transport. This means that further progress in improving transportation facilities, including high-speed land transport, is hardly possible without developing new economical means of controlling near-wall flows [1, 2]. The experience gained in the study of the possibility of decreasing the friction resistance of model objects by various methods within a period of several decades has allowed one to draw a number of practically important conclusions. Thus, the creation of a laminar form of flow only on the engine pod is capable of providing a decrease in the total aerodynamic drag of a subsonic transport airplane by 1–2% [3, 4]. The experience of controlling laminar flow is in this case a good starting point for developing effective methods for acting on a turbulent boundary layer. However, with its seeming simplicity, laminar flow is a challenging object of study at high Reynolds numbers. Thin laminar boundary layers are extremely sensitive to the streamlined surface defects that inevitably arise as a consequence of tolerances in manufacturing flying vehicles or appear because of the presence of joints and couplings of various aerodynamic elements, pollutions produced by insects, and defects arising as a result of collision of the fin leading edge, fuselage nose, and engine nacelles with sand particles and fine debris. It is clear that it is a not simple task to control such flows on transport aeroplanes.

In flow past many elements of flying vehicles such as the airplane fuselage and rocket body, the boundary layer is in a turbulent state in a wide range of Reynolds numbers. Therefore the use of artificial means of controlling turbulent flows, say, by blowing in gas [5–9] through a high-tech finely perforated permeable surface, seems to be one of the encouraging methods of decreasing the friction resistance and total aerodynamic drag for increasing the aerodynamic efficiency of a flying vehicle and, as a consequence, of increasing the flying range and useful load, reducing fuel costs and direct maintenance costs of it. In this connection, one more practical problem must be noted for the solution of which blowing-in (injection) of a fluid through a porous wall is used, that is, thermal protection of the surfaces subjected to the effect of high-enthalpy flows (gas turbine blades, combustion chamber walls, and other elements of a rocket engine) [10, 11] that allows one to control the wall temperature, retaining it within the limits of operating safety. Wide acceptance in modern technology is also gained by the methods of thermal protection of a streamlined surface with the use of gas blankets [12].

The present paper is a sequel to work [13] and is devoted to the study of the characteristics of an incompressible turbulent boundary layer on a flat surface with injection of air supplied through a hydraulically smooth finely perforated wall at the expense of the resources of an external confined flow. It is shown in [13] that this allows one to attain a 60% decrease in the surface friction. At the same time, a number of negative factors in the flow past an experimental model have been revealed

S. A. Khristianovich Institute of Theoretical and Applied Mechanics, Siberian Branch of the Russian Academy of Sciences, 4/1 Institutskaya Str., Novosibirsk, 630090, Russia; email: kornilov@itam.nsc.ru. Translated from Inzhenerno-Fizicheskii Zhurnal, Vol. 88, No. 6, pp. 1448–1459, November–December, 2015. Original article submitted December 17, 2014.

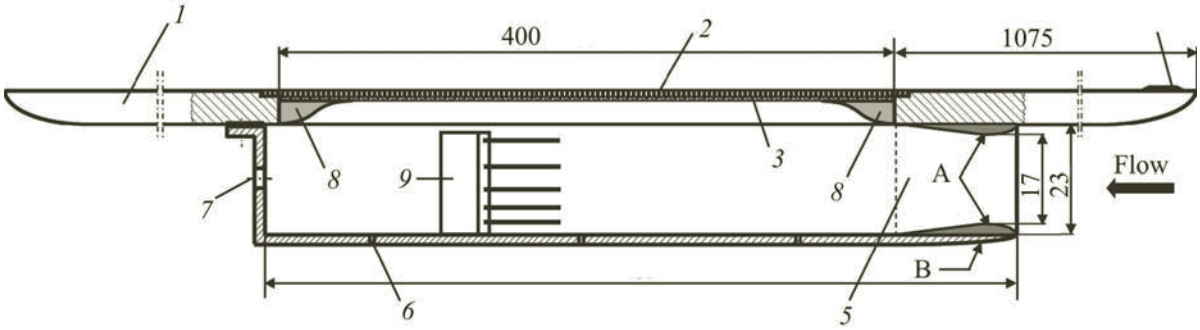

Fig. 1. Schematic diagram illustrating the model: 1) flat plate; 2) finely perforated sample; 3) fine-mesh filter; 4) boundary layer agitator; 5) input device; 6) pressure head; 7) regulated flaps of air passage; 8) fairing; 9) total pressure comb. All dimensions are not to scale, in millimeters.

such as, in particular, the presence of a nonstationary flow inside the input device, which requires modernization of the model and the corresponding check of the changes made.

Experimental and Computational Procedures. Experiments were carried out in a T-324 subsonic low-turbulent wind tunnel of the S. A. Khristianovich Institute of Theoretical and Applied Mechanics of the Siberian Branch of the Russian Academy of Sciences. The working section of the tunnel measured $1 \times 1 \times 4$ m^3, and the unperturbed flow velocities in the control section U_∞ were from 9 to 23 m/s, which corresponded to Reynolds numbers $\mathrm{Re}_1 = (0.60–1.53)\cdot 10^6$ m^{-1}.

Measurements were made on a model of a flat plate made from D16T Duralumin with dimensions 2204.5×993 mm^2 in plan and thickness of 6 mm (Fig. 1) positioned horizontally in the working section of the tunnel. Both the leading and trailing parts of the plate 1 on its idle side had the shape of a semi-ellipse with the ratio of its semi-axes b/a = 1:12. A number of static-pressure vents of diameter 0.4 mm were made on the symmetry axis of the plate. The trailing part of the plate was equipped with a regulated trailing-edge flap with a chord of 170 mm with the aid of which the flow in the vicinity of the nose was controlled. The pressure distribution on the remaining part of the plate was corrected by setting it at a small angle of attack (of the order of 10′). The construction of the plate allowed us to mount, flush to its main surface, a changeable plane, finely perforated sample 2 of thickness 1.1 mm of rather large size in plan (420×250 mm^2), which made it possible to control the local properties of flow (average velocity, friction, velocity pulsations) over a large length x. The permeability parameters selected for the perforated sample on the basis of the data of [14] and confirmed by the results of [15] can be found in [7].

In the process of the experiment, the pressurized air of the incident flow entered the input device of rectangular cross section located on the lower (idle) side of the plate directly under the perforated sample and from the latter it entered the boundary layer through a SEFAR PET 1500 150/380-34Y intermediate fine-mesh two-layer filter 3 and the perforated wall itself. The inside of the front part of the input device 5 represented a semi-profile, the shape of which is described by the relation

$$y = 30\,(0.2969\sqrt{\bar{x}} - 0.126\bar{x} - 0.3516\bar{x}^2 + 0.2843\bar{x}^3 - 0.1015\bar{x}^4)\,, \qquad (1)$$

where $\bar{x} = x/c$ and c is the semi-profile chord, equal to 50 mm. On the outside the front part of the device represented a semi-ellipse with the ratio of axes 1:33.

The choice of the geometry of the input device was based on three objectives: achievement of nonseparating flow at the inlet, and production of a high pressure in the flow section of the input device to ensure a maximum rate of air flow through the perforated surface, and as a result of the latter, increase in the efficiency of the device and ensuring uniform (over the area) injection of air into the boundary layer. To attain precisely these ends, the technical ledge at the joint of the perforated wall of the input device was eliminated by mounting a smooth fairing 8. The boundary layer on the working side of the plate was agitated artificially by mounting a 30-mm-long band covered by coarse calibrated sand with grain size h = 0.8 mm in the region of the maximum change in pressure (the vicinity of the leading edge).

Main measurements were made with the aid of a fully automated remotely controlled traverse gear with two degrees of freedom, x and y. The movement of the operational element of the traverse gear over the boundary layer height y was brought about by a preassigned program incorporating the choice of the needed step (up to 1 μm), as well of the needed

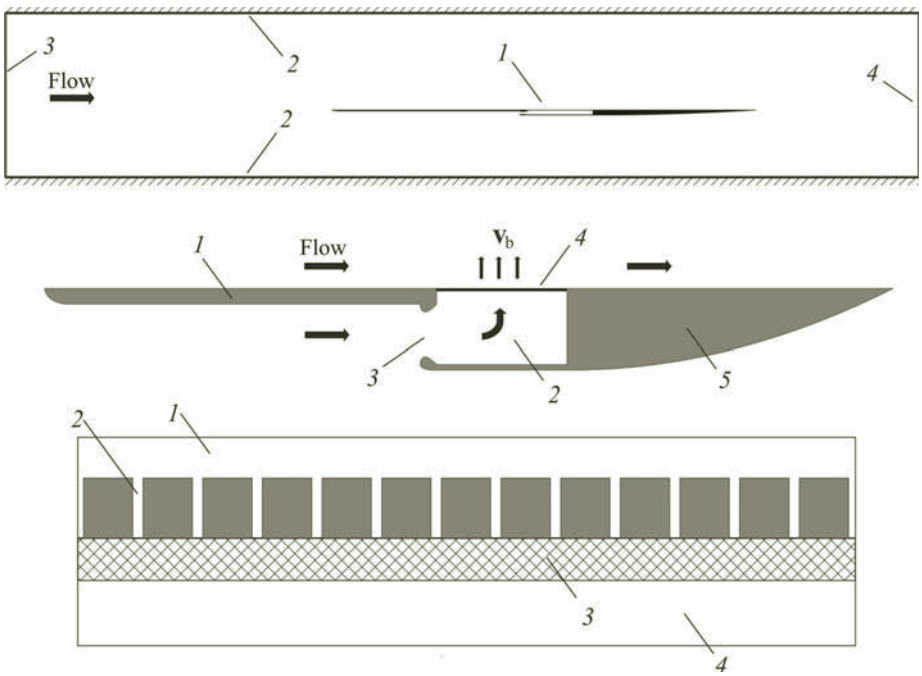

Fig. 2. Computational domain (a), geometry of the calculated model (b), and the model of perforated surface (c): (a) 1) plate; 2) ceiling and floor of the working section of wind tunnel; 3, 4) inlet and outlet boundaries; (b) 1) front part of the plate; 2) pressure chamber; 3) input device; 4) perforated sample; 5) rear part of the plate; (c) 1) flow region above the plate; 2) slits; 3) two-layer fine-mesh filter; 4) pressure chamber.

parameters for the acquisition of information on the average velocity fields and turbulence parameters. In this case, both the collection and processing of the information recorded in the course of experiments were done directly at the rate of the experiment and analyzed promptly by the program means developed on the basis of the MatLab package. The method of measuring an instantaneous velocity u at the analyzed point of the shear flow field with the use of a 55M0 system of hot-wire anemometric instruments of DANTEC Company is detailed out in [7]. We note only that as a primary transducer we used a miniature sensor known in the literature as the boundary layer probe with a sensitive element made from a tungsten filament of diameter 5 μm and length 1.2 mm that operated in the regime of constant temperature at 1.7-fold superheating.

The substantiation of the method of determining the local coefficient of surface friction C_f as a basic determining quantity in a noncanonical turbulent flow, which, in particular, can be formed in the presence of injection, is made in [16]. We note only that the method allows one to account for the cooling effect of the wall on hot-wire anemometer readings and to correctly describe the velocity distribution in the near-wall portion of the profile and, as a consequence, to determine C_f not only for the logarithmic portion of the velocity profile (when any), but also using, for the purpose, the region of the laminar sublayer of a turbulent boundary layer.

The total pressure P_0 in the flow passage of the input device was measured with the aid of a five-point mobile total-pressure comb 9 with feed openings countersunk at an angle of 60^o. Calibration of a single receiver in an unperturbed flow field has shown that within an error of 1% the region where it is insensitive to the angles of flow downwash does not exceed $\pm 23^o$. A random error in the determination of the most typical quantities, in particular, of the thicknesses of expulsion and loss of momentum $\sigma\delta^*$ and $\sigma\delta^{**}$, as well as of the local coefficient of surface friction σC_f, was found from the results of octuple measurements of the velocity profile in the boundary layer in the absence of injection and was equal to $\pm 3\sigma\delta^* = 0.9\%$, $\pm 3\sigma\delta^{**} = 0.84\%$ and $\pm 3\sigma C_f = 0.51\%$. A numerical solution of flow past a plate with an input device was made in a two-dimensional approximation with the aid of an ANSYS Fluent package. Use was made of the Reynolds-averaged two-dimensional Navier–Stokes equations for a viscous incompressible liquid. Launder–Spalding′s two-parametric differential k–ε model of turbulence [17] was employed for closing the system of equations.

Figure 2a shows a computational domain that constitutes a rectangle the upper and lower bases of which are the ceiling and floor of the wind tunnel working section 2, whereas the inlet and outlet boundaries 3 are located at distances

2000 mm and 1000 mm from the leading and trailing edges of the plate. At the inlet boundary we assigned the incident flow velocity U_∞, turbulence intensity ε_∞, and the ratio of turbulent viscosity to molecular one $\mu_{t\infty}/\mu_\infty$. The value of ε_∞ equal to 0.05% was selected from the measured data of flow velocity in the wind tunnel, and the ratio of viscosities equal to 1 was taken following the recommendations of the package developers according to which the values typical of a free-stream flow lie within the range $\mu_{t\infty}/\mu_\infty \approx 1$–10. Since the T-324 wind tunnel is a low-turbulent one, the low value of the range was selected. On the outlet boundary of the computational domain we assigned the reference values of static pressure (1 atm) and of total temperature (300 K), as well as the turbulence intensity and the ratio of the turbulent and molecular viscosities equal to the corresponding values in the incident flow. In carrying out calculations, all the flow parameters from the internal computational domain were extrapolated to the boundary except for the pressure that was calculated as a weighted-mean of the pressure inside the domain and for the reference pressure on the boundary by the method of five-order accuracy approximation.

The calculated model (Fig. 2b) includes the forepart of the plate 1 located before the perforated sample 4, pressure chamber 2, input device 3, the sample itself 4 with a permeable backing (filter) under it, and the rear part of the plate 5. The geometries of the computational and aerodynamic models are identical in principle except for the lower part 5 where, in contrast to the experimental model, there was a smooth transition from the rear part of the pressure chamber to the trailing edge of the model.

To simply the problem, the perforated wall was replaced by a surface with 400 transverse slits uniformly spaced along x at intervals of 1 mm (Fig. 2c). The width of a slit corresponds to the diameter of an individual hole (pore) and is equal to 0.17 mm. The distance between the slits was selected proceeding from the condition of the equality between the coefficients of porosity for real and computed plates. Figure 2c shows the region of flow above plate 1, slits 2, two-layer fine-mesh filter 3 of thickness 0.7 mm, and pressure chamber 4. Air was blown into the boundary layer above the perforated plate because of the pressure drop between regions 4 and 1.

Since the speed of air injection is small, the flow across the fine-mesh porous filter was assumed laminar and was calculated with the use of the Darcy equation $\nabla P = -k\mu \mathbf{v}_{\text{ref}}$, where ∇P is the pressure gradient along the streamline, $\mathbf{v}_{\text{ref}}$ is the volume velocity vector at the reference point inside the porous volume, μ is the coefficient of molecular viscosity of air, and k is the coefficient of the hydraulic resistance of pores. The volume velocity was determined as $\mathbf{v}_{\text{ref}} = \varphi \mathbf{v}$, where $\mathbf{v}$ is the vector of average velocity in the pore channel, and φ is the porosity factor of the material; it represents the ratio of the volume occupied by air in a porous material to the total volume of this material. The values of the parameters $k = 3.07 \cdot 10^{11}$ m^{-2} and $\varphi = 0.5$ were selected from the condition of the equality between the calculated and experimental values of the hydraulic resistance of the perforated plate–two-layer filter (located under the plate) combination.

The computational grid is constructed near the model so that the laminar sublayer of the turbulent boundary layer could be resolved explicitly. For this purpose, we refined the grid in the direction of the coordinate y transverse to the wall, as a result of which y^+ was equal approximately to 0.2. In the vicinity of the slits, the grid was constructed so that the width of each slit could comprise 10 computational cells, with 25 cells in the space between the slits. Such splitting made it possible to obtain a detailed distribution of the friction factor on the perforated plate surface and also between the slits. To compare the experimental data with the results of numerical calculation, the value of the friction factor was averaged on each portion of the perforated plate between neighboring slits. The entire computational domain contained 5.5 million of rectangular cells, of which 2.5 million were located above the perforated plate, 2.1 million inside the pressure chamber, 120 thousand in the region occupied by the slits, with 300 cells per slit, 84 thousand on the filter, with 0.7 million cells for the remaining computing space.

Results of Investigations. Characteristics of the Initial Boundary Layer. The character of change of the static pressure in the flow regions located upstream and downstream of the perforated sample shows that in the indicated regions (except for the vicinities of the leading and trailing edges of the plate) there are portions of practically nongradient flow, where the static pressure can be considered almost constant within the experimental error.

The local and integral properties of flow directly in the boundary layer show that the characteristics of the shear flow on the perforated surface correspond to the physical representations of the properties of a turbulent boundary layer being formed on an impermeable smooth flat plate in the case of a nominally nongradient flow past it. For example, the distributions of the integral characteristics of a boundary layer, in particular, of the thicknesses of expulsion δ^* and loss of momentum δ^{**}, reveal the flow properties close to the standard ones.

Figure 3 presents the dependence $C_f = f(\text{Re}^{**})$ that characterizes the change in the local coefficient of surface friction C_f with the Reynolds number Re^{**}. The data of calculations by the formula from [18] for a smooth flat plate immersed in a nongradient flow are also presented in this figure for comparison:

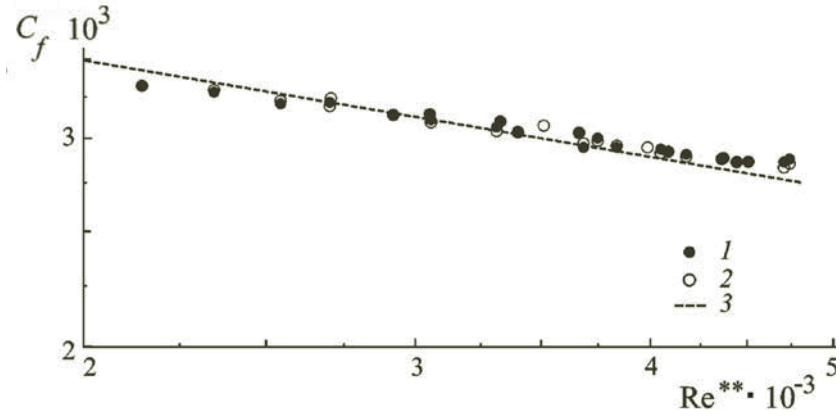

Fig. 3. Local coefficient of surface friction C_f vs. the Reynolds number Re^{**} without air passage: 1) calculation with the use of the wall law for the logarithmic region of the boundary layer; 2) calculation by the procedure suggested by the present authors [16]; 3) calculation by formula (2).

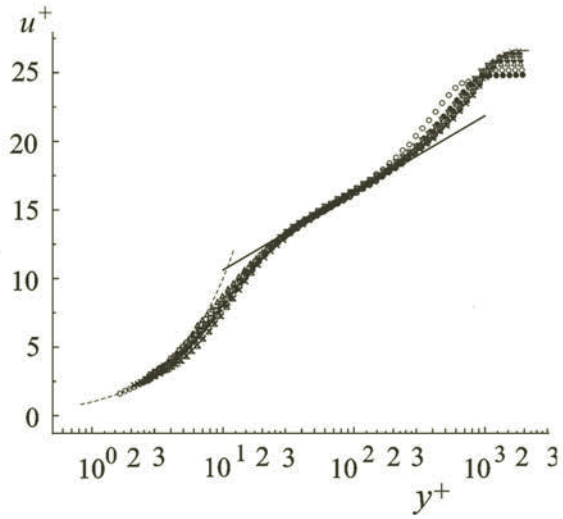

Fig. 4. Average velocity profiles in a boundary layer in the variables of the wall law without air passage: points, experiment at $\mathrm{Re}_x = (1.278–2.541)\cdot 10^6$; solid line, $u^+ = 5.62y^+ + 5.0$; dashed line, $u^+ = y^+$.

$$C_f = \frac{0.3e^{-1.33H}}{(\log \mathrm{Re}^{**})^{1.74+0.31H}}. \qquad (2)$$

On the whole, there is quite a satisfactory agreement between the experimental values of C_f obtained by two methods and the results of calculations by formula (2). Some discrepancy is observed at the ends of the interval. However, the maximum deviation of the experimental values of C_f from the calculated ones, including from those obtained on the permeable surface itself, does not exceed 4%. This result directly supports the important fact that flow past a finely perforated wall in the absence of a stream through the input device is practically equivalent to flow past a hydraulically smooth analog.

As regards the internal region of the turbulent boundary layer, the behavior of the local characteristics of flow in this region can be considered using as an example the velocity profiles obtained along the length of the model and presented in Fig. 4 in the coordinates of the wall law $u^+ = f(\log y^+)$:

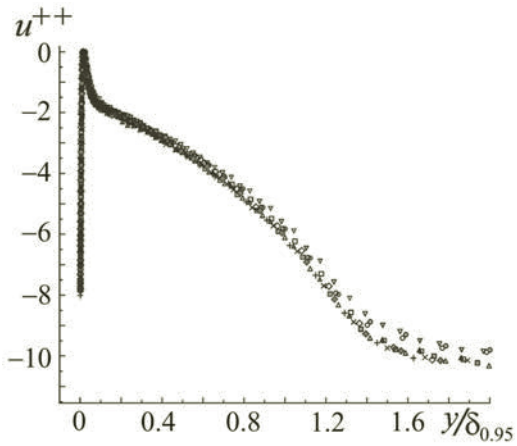

Fig. 5. Profiles of the longitudinal component of velocity pulsations in a boundary layer without air passage at $\mathrm{Re}_x = (1.278–2.541)\cdot 10^6$.

$$u^+ = u/v_* , \quad y^+ = yv_*/\nu .$$

It is seen that in the absence of air stream through the input device, the velocity distribution in the logarithmic region of the boundary layer is quite satisfactorily described by the classical velocity profile $u^+ = A \log y^+ + B$ with the coefficients $A = 5.62$ and $B = 5.0$ [19].

The profiles of the turbulent pulsations of velocity in the boundary layer also confirm the fact that in this case the characteristics of a shear flow above a perforated wall are not at variance with the physical notions about the properties of a turbulent boundary layer formed on a smooth flat plate under conditions of nongradient flow. We only note that in contrast to [21, 21] where the scale $U_\infty \delta^*/\delta_{99}$ was used for the average velocity to describe the flow properties in the external region of the boundary layer, we have proposed a technique of normalization of the integral intensity of velocity pulsations in the form

$$u^{++} = (u' - u'_{\max})/(u'_{\max})\delta^*/\delta_{95} = f(y/\delta_{95}) ,$$

where $u'_{\max}$ is the maximum value of velocity pulsations in the section of measurements. The results obtained in this way are presented in Fig. 5. As is seen, the profiles of velocity pulsations in the boundary layer of the plate (also over its permeable part) normalized with the use of the above-indicated scale are generalized with sufficient accuracy by a single dependence. It is natural that this technique of normalization cannot be extended to more general cases of flow and, as a minimum, requires verification in an extended range of Reynolds numbers and flow velocities.

Results of Investigations. Characteristics of Flow in the Presence of Air Passage through the Input Device. At the initial stage of experiments, it was elucidated that the nonstationary character of the stream revealed in the flow passage of the input device in the previous series of experiments was caused by the formation of a transient regime of flow on the idle side of the plate. In this connection further experiments were carried out in conditions under which the boundary layer was also agitated artificially. We note immediately that this technique has been fully justified. Moreover, a fine-mesh wire net set up at the inlet to the input device and a metallic felt with a random porous microstructure, not used in this series of experiments, aid in weakening the nonstationary effect.

Figure 6 presents as an example the distributions of the pressure coefficient $C_p = (P_0 - P_\infty)/q_\infty$ along the coordinate y on the idle side of the model measured at different distances from the leading edge of the input device along the coordinate x. The process of the boundary layer build-up in the direction of the coordinate x is clearly seen; its thickness before the inlet into the flow passage ($x = –60$ mm) exceeds 20 mm. The estimation of the boundary larger thickness on the basis of the well-known classical formulas shows that a turbulent flow is implemented here. Also noteworthy is the pressure constancy in the very flow passage ($x = 120–375$ mm) except for its initial portion ("throat") ($x = 14.5$ and 45.7 mm). The pressure coefficient in this case on the lower wall of the input device (cross) practically does not differ from the corresponding values of C_p in the flow section. This points to a rather uniform character of stream inside the input device.

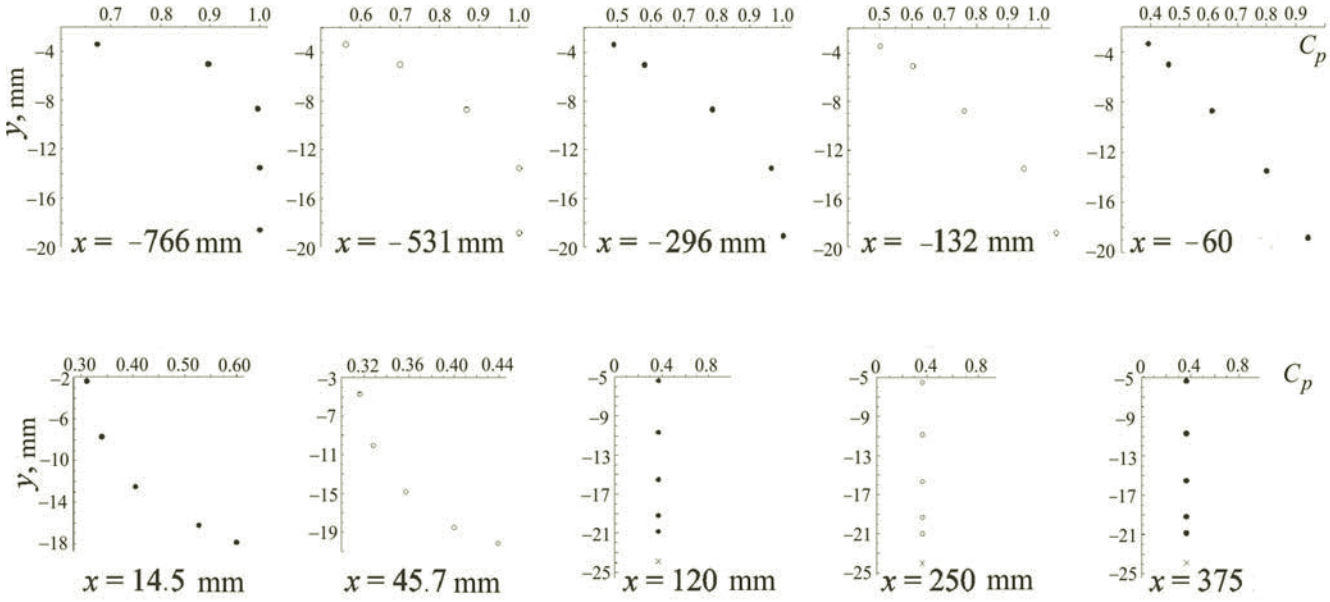

Fig. 6. Profiles of total pressure coefficient $C_p = f(y)$ on the idle side of the model with air passage.

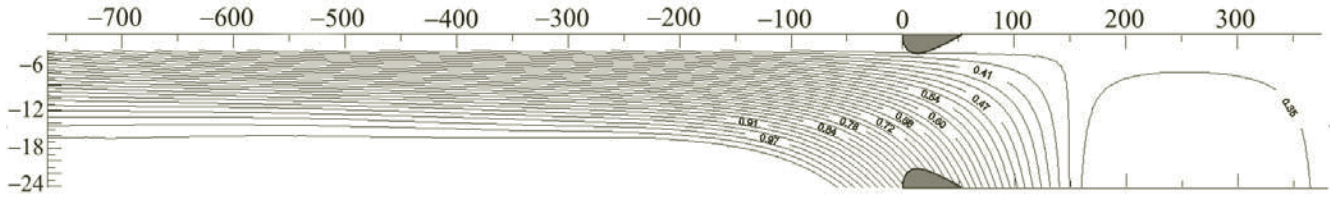

Fig. 7. Lines of equal values of the coefficient total pressure C_p = const on the idle side of the model with air passage.

Figure 7 shows the lines of equal values of the coefficient of total pressure C_p = const on the idle side of the model. The lack of detailed data for the external side of the input device does not make it possible to obtain the full picture of flow past this device. At the same time it is seen that the distribution of the isolines C_p = const contains nothing unusual and corresponds well to the physical notions about the character of the flow under study.

The profile of the average flow velocity in the boundary layer above the perforated surface in the presence of air stream through the input device has in principle the same form as in the case of forced air delivery into the pressure chamber [7]. In particular, the distribution of the average flow velocity in the internal region of the boundary layer reveals a distinct deviation of the experimental relation $u^+ = f(y^+)$ from the classical law of wall (profile 2 in Fig. 8). Since the wall law variables u^+ and y^+ are scaled by the dynamic velocity x_*, it is clear that this fact points indirectly to the substantial decrease in friction and is indicative of the tendency typical of forced blowing.

The profiles of turbulent pulsations of the velocity u' are given in Fig. 9 in the form of the dependence $u^{++} = f(y/\delta_{95})$, i.e., with application of the same technique of normalization as that used for the initial flow (Fig. 6). This figure contains only those profiles that were measured in the region of flow stabilization, where the main characteristics of flow (for example, C_f) become linear in the direction of the x axis. Analysis of all available data shows that the mismatch between the profiles of u' increases with the distance from the stabilization region. However, in our opinion, the given example gives us good reasons to claim that the profiles (normalized with the use of such a scale) of velocity pulsations over the permeable part of the plate in the region of flow stabilization and in the presence of air passage can be described by a single dependence with satisfactory accuracy.

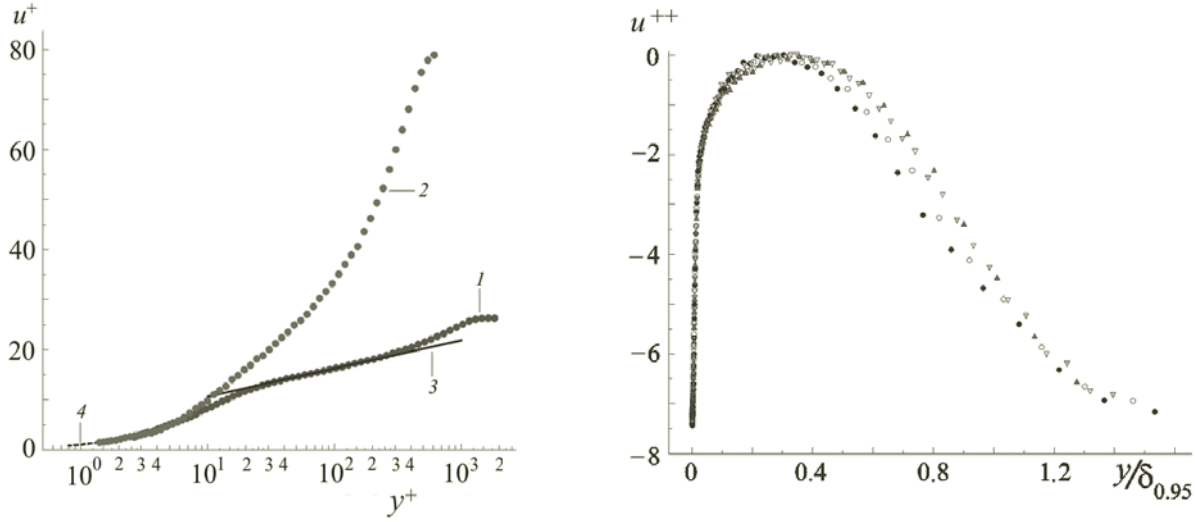

Fig. 8. Average velocity profiles in a boundary layer in the variables of the wall law without air passage (1) and with air passage (2) at $\mathrm{Re}_x = 2.059 \cdot 10^6$; 3) $u^+ = 5.62y^+ + 5.0$; 4) $u^+ = y^+$.

Fig. 9. Profiles of the longitudinal component of velocity pulsations in a boundary layer with air passage at $\mathrm{Re}_x = (1.996–2.205) \cdot 10^6$.

Air injection through the input device with regulated flow rate (on variation of the external forced flow velocity) can be considered as a means of action on the state and characteristics of a turbulent boundary layer on a streamlined surface. Therefore of definite interest is the efficiency of such a method of control. In the first approximation this efficiency can be estimated on the basis of the computational-experimental data on friction distribution. Figure 10 presents the results of measurements of the experimental values of the coefficient of surface friction $C_f/C_{f0} = f(x/L)$, where C_{f0} represents the corresponding values of the friction factor in the initial flow (points) along the flat plate with air passage through the input device. It is seen that on the whole the data of numerical calculation, at least above the perforated surface and ahead of it, qualitatively correctly reflect the character of change in the dependence $C_f/C_{f0} = f(x/L)$. We note also the substantial decrease in the coefficient of surface friction, as is seen from the experimental and calculated data. It has been possible to attain the greatest decrease in friction at the end of the perforated sample, where the difference from the initial flow, defined as $\Delta C_f/C_{f0}$, attains 85%. It is seen from the character of the behavior of the dependence $C_f/C_{f0} = f(x/L)$ that the region of the lowered values of C_f/C_{f0} encompasses not only the perforated surface itself, but propagates downstream to the impermeable part of the plate. Moreover, as opposed to the data of numerical calculation, where the distribution of C_f in the indicated region is of asymptotic character, the experimental results do not disclose such a dynamics. The difference between the calculation and experiment in the indicated flow region is attributed to the following reasons.

Under the conditions studied, the local flow velocity that is normal to the wall and that accounts for fractions of a percent of the incident flow velocity U_∞ is rather small. At the same time, the cumulative effect caused by the natural thickening of the boundary layer in the direction of the x axis and due to injection must promote the turning of the velocity vector above the perforated surface in the direction of the external flow. As the shear flow reaches the permeable wall-impermeable wall interface, the normal velocity component disappears altogether, which leads to the collapse of flow with formation of a rolling-type vortex with the angular rotational velocity ω_z. This in turn slows down the rate of increase in the surface friction in some limited region of flow located behind the perforated sample. As the longitudinal coordinate x increases, the intensity of the vortex becomes weaker, and finally it disappears altogether, since there are no energy sources to feed it. As a consequence, C_f gradually attains the corresponding value close to its equilibrium state. A similar phenomenon appears also on the frontal impermeable wall–permeable wall interface. The difference lies however, in the fact that the collapse of flow with the formation of a rolling vortex occurs on the very perforated surface, i.e., in the region of active injection. It is clear that in this case such a phenomenon, at least in a limited region of flow, must favor an additional decrease in surface friction.

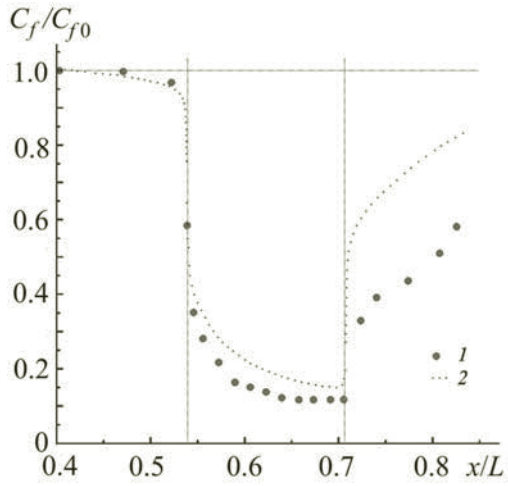

Fig. 10. Distribution of the normalized coefficient of surface friction along the length of the model: points, experiment; dotted line, numerical calculation.

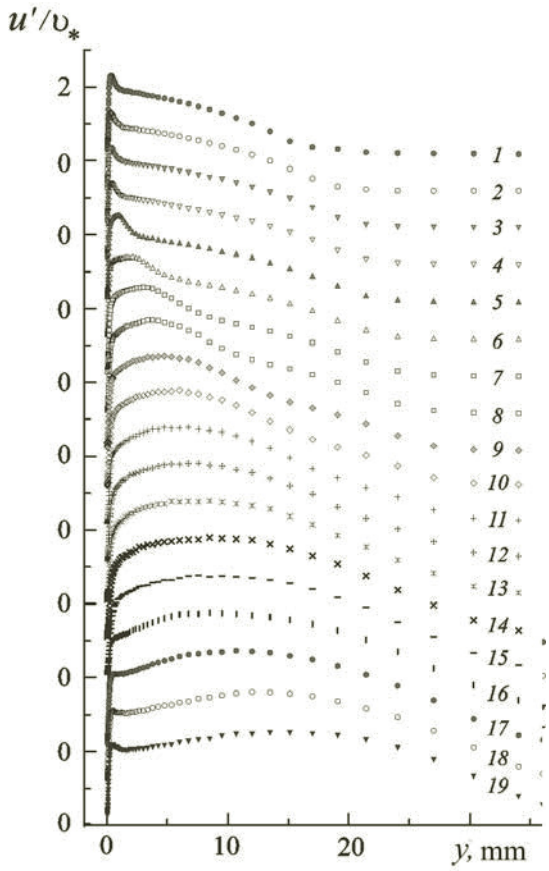

Fig. 11. Profiles of the longitudinal component of velocity pulsations in a boundary layer along the length of the model at Re_x = $1.248 \cdot 10^{-6}$ (1), $1.459 \cdot 10^{-6}$ (2), $1.617 \cdot 10^{-6}$ (3), $1.669 \cdot 10^{-6}$ (4), $1.690 \cdot 10^{-6}$ (5), $1.721 \cdot 10^{-6}$ (6), $1.773 \cdot 10^{-6}$ (7), $1.825 \cdot 10^{-6}$ (8), $1.877 \cdot 10^{-6}$ (9), $1.929 \cdot 10^{-6}$ (10), $1.981 \cdot 10^{-6}$ (11), $2.037 \cdot 10^{-6}$ (12), $2.085 \cdot 10^{-6}$ (13), $2.141 \cdot 10^{-6}$ (14), $2.184 \cdot 10^{-6}$ (15), $2.241 \cdot 10^{-6}$ (16), $2.293 \cdot 10^{-6}$ (17), $2.396 \cdot 10^{-6}$ (18), and $2.500 \cdot 10^{-6}$ (19).

The second reason for the above-mentioned difference lies in the formation of an essentially new flow downstream from the rear permeable wall–impermeable wall interface. Indeed, from Fig. 11, which presents the profiles of the integral intensity of velocity pulsations $u'/v_* = f(y)$ along the length of the model, interesting conclusions can be drawn. Upstream from the perforated portion (distributions 1–4), the profiles of pulsations have the character typical in principle of the classical turbulent boundary layer, which is quite natural. As the longitudinal coordinate x increases (distributions 5–14), the maximum of velocity pulsations increases somewhat in absolute magnitude and is gradually displaced to the side of the external edge of the boundary layer. Here, we observe the same characteristic distribution of u' over the boundary layer height as that revealed by us earlier in the case of forced injection of air through the pressure chamber, namely, the presence of at least two, as a minimum, flow regions: a region with lowered (as compared with the initial flow) values of u' directly near the wall and a region with increased values of u' at a distance from the wall. In the former case, this points to the fact that in the presence of passage through the input device the maximum of the turbulent velocity pulsations is forced back from the wall, indicating the thickening of the viscous sublayer and, as a consequence, a decrease in the surface friction. Thus, here there exist nearly the same tendencies that are typical of forced blowing-in. With further increase in the longitudinal coordinate x (distributions 15–19), slow relaxation of flow characteristics occurs on the impermeable part of the surface to the state of complete hydrodynamic equilibrium with formation of a distinctly expressed maximum of pulsations directly near the wall. This is indicative of the generation of a new layer that usually appears in flow past various kinds of surface irregularities, protrusions, and obstacles behind which a typical relaxation process takes place [22]. The indicated circumstances have not so far been included in the scheme of numerical calculation. Moreover, within the framework of the present research, we failed to reflect, with acceptable accuracy, the value of injection intensity that could play the role of the initial parameter in the algorithm of calculation and that would be adequate to the value of the injection coefficient in the experiment.

The above-mentioned extensive region of flow characterized by lowered values of friction behind the active region of injection is of importance for the balance of the total aerodynamic drag of the plate–input device combination. Indeed, the resistance coefficient C_x of the investigated model configuration represents the sum of the external coefficient of resistance C_{xw} determined by the loss of momentum in the boundary layer, of the internal coefficient of resistance ΔC_x equivalent to the power consumed in the process of injection, the coefficient of resistance of the input device itself $C_{x\text{inl}}$, and of the interference component $\Delta C_{x\text{int}}$ of the plate–input device combination:

$$C_x = C_{xw} + \Delta C_x + C_{x\text{inl}} + \Delta C_{x\text{int}} . \tag{3}$$

The first component of the total resistance is determined from the results of integration of the dependence $C_f = f(x)$ along the plate, which does not involve great difficulties. Since the integration limits include also the region of flow behind the perforated sample, it is evident that an additional gain in the resistance is achieved in this case. As for the second component, here there are certain difficulties as there are no accurate data on the value of the mass rate of flow of gas Q through the perforated plate that can be determined as

$$Q = \gamma F V_{\text{av}} ,$$

where F is the "useful" free area of the permeable sample and V_{av} is the average (over the sample area) velocity of injection. The value of V_{av} can be determined from the Darcy law:

$$V_{\text{av}} = \sqrt{\frac{2\Delta P}{\rho\zeta}} ,$$

where ΔP is the averaged pressure difference between the flow passage of the input device and the static pressure of the incident flow and ζ is the coefficient of hydraulic resistance of the perforated plate–two-layer filter (lying under the plate) combination determined by calibration. For this purpose, a tested multilayer sample was placed in a specially manufactured dismountable part of a DISA Type 55D41/42 device. In the process of measurements we controlled the drop in the total pressure due to the pressure loss on the sample and the flow parameters at the inlet of the working section. The results obtained are presented in Fig. 12 in the form of the dependence $\zeta = f(\text{Re}_\delta)$, where Re_δ is the Reynolds number based on the overall thickness of the sample. It is seen from this figure that the coefficient of hydraulic resistance decreases with increase in Re_δ, which agrees completely with the data for obstacles uniformly distributed over the section (networks, honeycomb, and other gears) [23]. Meanwhile this information is inadequate, since, strictly speaking, the "useful" free area of the permeable sample F is unknown as the sample is a multilayer construction with mutually overlapping holes. Thus, with such an approach the average velocity of injection V_{av} and, consequently, the coefficient of injection cannot be determined accurately enough.

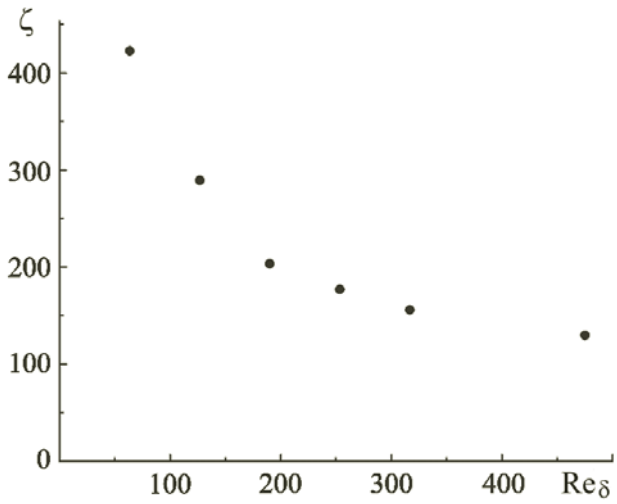

Fig. 12. Coefficient of hydraulic resistance of the perforated plate–fine-mesh filter combination vs. the Reynolds number.

As regards the third component and especially the contribution made to the total resistance due to the interference of the plate–input device combination (the fourth component in Eq. (3)), their determination is still more complex. Therefore henceforth it would appear reasonable to adjust the procedure of gravimetric experiment such that one could measure the total aerodynamic drag of the model configuration with an operating input device.

CONCLUSIONS

1) The use of the resources of the external confined flow for organization of air injection through a finely perforated wall is quite a fully justified technique for studying the local and integral characteristics of a turbulent boundary layer on a streamlined surface, since it is a simple, accessible, and reliable means of effect on a studied flow under conditions of aerodynamic experiment.

2) In using the proposed technique, there is no need for forced air supply, which allows one to avoid encumbering the working section of a wind tunnel with additional devices and makes it a simple instrument for studying the efficiency of air injection into a boundary layer from the viewpoint of decreasing the friction of a streamlined surface. Within the framework of the approach used, a stable decrease in the local values of the coefficient of surface friction along the length of the model has been revealed that may attain more than 85% at the end of the perforated portion.

3) It is advisable to extend the proposed technique to measuring the total aerodynamic drag of the flat plate–input device configuration, which would make it possible to judge the aerodynamic efficiency of the considered method of the effect on a boundary layer including the possibility of improving the configuration of the passage of the very input device. Significant attention is to be also devoted to the necessity of accurate determination of the characteristics of the rate of flow through the flow passage.

4) The generalization of experimental data on the distribution of the longitudinal component of velocity pulsations in a boundary layer with the use of the scales $u'_{\max}$ and δ^*/δ_{95} can be considered only as a starting point for a subsequent more detailed analysis. It is clear that here a scale for the velocity of injection must also be involved.

5) Notwithstanding the fact that many aspects of injection through a permeable surface are known today, the problem of more general character, which is connected with the necessity of seeking an optimal geometry, permeability degree, and of the mutual disposition of holes, as well as of other parameters of holes and their relationship with the characteristic scale of flow, remains little understood.

6) The results of the numerical calculations carried out qualitatively correctly reflect the change in the local parameters of a turbulent boundary layer above a perforated surface, including friction, in the case of air injection by supplying an external confined flow. At the same time, further advance in the solution of this problem is possible only by developing more perfect calculation algorithms that allow taking into account the specific features of flow at the permeable wall–impermeable wall interface.

NOTATION

$C_b = \rho v_b/\rho U_\infty$, average (over the area) coefficient of injection; C_f, local coefficient of surface fiction; C_x, coefficient of aerodynamic drag; $H = \delta^*/\delta^{**}$, form parameter of a boundary layer; $\mathrm{Re}_1 = U_{\infty 1}/\nu$, single Reynolds number, m^{-1}; $\mathrm{Re}^{**} = U_\infty \delta^{**}/\nu$, Reynolds number based on δ^{**}; U_∞, flow velocity in the control section, m/s; $u^+ = u/v_*$, dimensionless flow velocity; u', root-mean-square value of the longitudinal component of flow velocity pulsations, m/s; v_b, injection velocity, m/s; $v_* = (\tau_w/\rho)^{1/2}$, dynamic velocity of air flow, m/s; $y^+ = yv_*/\nu$, dimensionless coordinate; δ_{95}, boundary layer thickness determined from the condition $U/U_\infty = 0.95$ mm; δ^* and δ^{**}, thicknesses of expulsion and loss of momentum, mm; ν, kinematic coefficient of viscosity, m^2/s; ρ, air density, $\mathrm{kg\cdot s}^2/\mathrm{m}^4$; τ, shear stress, $\mathrm{kg/m}^2$.

REFERENCES

1. R. Wood, Impact of advanced aerodynamic technology on transportation energy consumption, *SAE Int. TP-2004-01-1306* (2004).
2. A. Abbas, J. de Vicente, and E. Valero, Aerodynamic technologies to improve aircraft performance, *Aerospace Sci. Technol*., **28**, 100–132 (2013).
3. W. K. Lord, S. H. Zysman, T. G. Tillman, and W. A. Johnson, *Laminar Flow Control Experiment on a Large-Scale Nacelle Model*, Pratt & Whitney Report PWA 6420-55, December 1995.
4. B. Barry, S. J. Parke, N. W. Brown, H. Riedel, and M. Sitzmann, The flight testing of natural and hybrid laminar flow nacelles, *ASME Paper 94-GT-408*, June 1994.
5. D. Hwang, Review of research into the concept of the microblowing technique for turbulent skin friction reduction, *Prog. Aerospace Sci*., **40**, 559–575 (2004).
6. T. G. Tillman and D. P. Hwang, Drag reduction on a large-scale nacelle using a microblowing technique, *37th AIAA Aerospace Sci. Meeting and Exhibit*, Reno, NV, *AIAA Paper 1999-0130*, January 1999.
7. V. I. Kornilov and A. V. Boiko, Efficiency of air microblowing through microperforated wall for flat plate drag reduction, *AIAA J*., **50**, No. 3, 724–732 (2012).
8. Y. L. Lin, M. K. Chyu, T. I. P. Shih, B. P. Willis, and D. P. Hwang, Skin friction reduction through micro-blowing, *AIAA Paper*, No. 0359 (1998).
9. J. Li, C.-H. Lee, L. Jia, and X. Li, Numerical study on the flow control by micro-blowing, *47th AIAA Aerospace Sci. Meeting*, Orlando, FL, *AIAA 2009-779*, January 2009.
10. F. A. P. Silva, D. O. A. Cruz, and C. C. Pellegini, Velocity and temperature distributions in compressible turbulent boundary layers with heat and mass transfer, *Int. J. Heat Mass Transf*., **38** (13), 2507–2515 (1995).
11. J. Bellettre, F. Bataille, and A. Lallemand, Prediction of thermal protection of walls by blowing with different fluids, *Int. J. Therm. Sci*., **38**, 492–500 (1999).
12. S. S. Kutateladze and A. I. Leontiev, *Heat/Mass Transfer and Friction in a Turbulent Boundary Layer* [in Russian], Énergoatomizdat, Moscow (1985).
13. V. I. Kornilov, A. V. Boiko, and I. N. Kavun, Control of a turbulent boundary layer by air injection on account of the external flow resources, *Teplofiz. Aéromekh*., **22**, No. 4, 429–443 (2015).
14. D. Hwang (I. Grant Ed.), Experimental study of characteristics of micro-hole porous skins for turbulent skin friction reduction, in: *Proc. 23rd Congr. Int. Council Aeronautical Sci.*, Optimage Ltd., Toronto, Canada (2002), pp. 2101.1–2101.7.
15. A. V. Bazovkin, V. M. Kovenya, V. I. Kornilov, A. S. Lebedev, and A. N. Popkov, Effect of micro-blowing of a gas from the surface of a flat plate on its drag, *J. Appl. Mech. Tech. Phys*., **53**, No. 4, 490–499 (2012).
16. A. V. Boiko and V. I. Kornilov, Measurement of the local coefficient of surface friction by a hot-wire anemometer, *Teplofiz. Aéromekh*., **17**, No. 4, 613–623 (2010).
17. B. E. Launder and D. B. Spalding, *Lectures in Mathematical Models of Turbulence*, Academic Press, London–New York (1972).
18. F. M. White, *Viscous Fluid Flow*, 2nd edn., McGraw-Hill, New York (1991).
19. D. E. Coles and E. A. Hirst (Eds.), Computation of turbulent boundary layer, in: *Proc. Stanford Conf. AFOSR-IFP*, Vol. 2, Stanford (1968–1969).
20. M. V. Zagarola and A. J. Smits, A new mean velocity scaling for turbulent boundary layers, in: *Proc. 1998 ASME Fluids Engineering Division Summer Meeting*, June 21–25, Washington D. C. (1998), pp. 1–6.

21. R. B. Cal and L. Castillo, Similarity analysis for transpired turbulent boundary layers subjected to external pressure gradients, *AIAA J*., **43**, No. 9, 1913–1922 (2005).
22. V. I. Kornilov and D. K. Mekler, Characteristic features of the development of a nonequilibrium boundary layer downstream of a cylinder immersed in a transverse flow, *Izv. Sib. Otd. Ross. Akad. Nauk SSSR*, *Ser. Tekh. Nauk*, Issue 6, 38–46 (1989).
23. I. E. Idel′chik, *Handbook on Hydraulic Resistances* [in Russian], Mashinostroenie, Moscow (1975).